Uncertainty in remaining orbital lifetime estimation after post-mission disposal

Lucía Ayala Fernández
Technische Universität Braunschweig
Carsten Wiedemann
Technische Universität Braunschweig

Vitali Braun
IMS Space Consultancy GmbH at ESA/ESOC

Stijn Lemmens
ESA/ESOC

ABSTRACT

A precise estimation of the orbital lifetime after the mission of a space object has ended is essential for space debris mitigation practices. In this paper, the accuracy of current standard practices applied to rocket bodies is investigated. The results are analyzed for two orbital regimes, Low Earth Orbit (LEO) and Highly Eccentric Orbits (HEO), and for different solar and geomagnetic activity scenarios. Furthermore, two different hypotheses were tested for the drag coefficient.

The results show the different dynamics and errors that can be expected for LEO and HEO objects, as well as different behaviors depending on the chosen solar and geomagnetic activity scenario and recommendations for the drag coefficient to be used. Moreover, specific examples are shown for LEO and HEO objects, in order to describe different dynamics that can lead to large errors in each orbital regime.

1. INTRODUCTION

One of the essential aspects of space debris mitigation is the performance of Post-Mission Disposal (PMD) once the mission of a space vehicle has concluded. The main goal of the PMD is to avoid the creation of further space debris, especially mitigating the risk of on-orbit collisions or explosions that would cause a fragmentation and potentially contribute to the collisional cascading effect known as the Kessler syndrome. An integral part of the PMD is the clearance from the protected regions, as it is stated in the IADC space debris mitigation guidelines [3]. For the Low Earth Orbit (LEO) protected region, this implies the re-entry into Earth's atmosphere within 25 years after the end of the mission.

In this context, orbital lifetime estimations are crucial to assess the compliance of new missions to be launched. Different standards provide guidance in the methodologies that can be applied for the orbit propagation leading to such estimates, such as [2, 16]. Even further, orbital lifetime estimations are also important for studies that analyze the current state of the orbital environment, which are essential to act accordingly and protect its sustainability. A good example is the Space Environment Report published yearly by the European Space Agency (ESA) [12]. This paper assesses the accuracy of the estimated orbital lifetime of rocket bodies following the standard procedures and tools from ESA [16]. The data used was extracted from DISCOS (Database and Information System Characterising Objects in Space), and divided in two distinct orbital regimes, objects resident in LEO and Highly-Eccentric Orbits (HEO), as very different dynamics can be observed in each of them.

The driving perturbation leading to the re-entry of objects in the LEO region is the drag force. A number of uncertainties influence the computation of the drag force acting on an object in space: the physical characteristics of the object, the attitude in which it is flying and the atmospheric density, which is influenced by the solar and geomagnetic activity (which are not known when propagating into the future), and inaccuracies of the atmospheric model that is used. For this reason, the results were analyzed for different solar and geomagnetic activity scenarios and for different values of the drag coefficient of the objects.

On the other hand, the dynamics in HEO orbits are more complicated than in LEO. Even though drag is still a force to be considered, due to the large eccentricity, other forces become also relevant, such as gravitational third body perturbations coming from the Moon and the Sun and solar radiation pressure. These complex dynamics represent a big challenge for the estimation of the orbital lifetime of objects in these orbits, as they are very sensible to changes in the initial conditions [11, 14]. As an example of the complex dynamics encountered in HEO, [4] states that the lifetime of an object in a 36,000 km $\times$ 250 km orbit (apogee $\times$ perigee) can vary from 8 years to 70 years just by varying the orientation of the orbit.

The scope of this paper was defined to include only rocket stages, in this context often referred as Rocket Bodies (RBs). RBs are a very distinct type of space objects for several reasons: firstly, their mission typically ends very shortly after reaching orbit, which makes their orbits easier to analyze. Moreover, they tend to have a similar shape, which can be approximated by a cylinder (even though it often includes a ”cone” attached). These shared characteristics make the RBs a suitable target group for this study. Additionally, many of the heaviest objects among the space debris population are RBs, and they are also the main source of on-orbit fragmentations [9]. This highlights the importance of assessing space debris mitigation practices for this kind of objects.

Similar studies to the one in this paper have already been performed in [7, 13]. The former study, however, only includes objects resident in the LEO region, and the latter considers one single solar and geomagnetic activity scenario. Furthermore, both studies perform the analysis assuming a default drag coefficient of 2.2 for all objects. The current paper will therefore update the studies presented in [7, 13] including newer data and using updated tools, but it will also analyze the uncertainty sources more in depth and will put a stronger emphasis in objects in HEO orbits, which have shown to be incredibly challenging. A different assumption for the drag coefficient of these objects will also be tested, in addition to the traditional default of 2.2. Finally, case studies will be presented for both orbital regimes, in order to describe some behaviors that lead to large errors in the orbital lifetime estimations.

2. METHODOLOGY

2.1 Dataset

The dataset used was extracted from the DISCOS database. In order to select the objects relevant for the study, the following characteristics had to be met:

1. Object type is RB.
2. The perigee of the object is below 2,000 km altitude.
3. The object has already re-entered, i.e. it has a registered re-entry epoch.
4. The object had been orbiting Earth for at least 1 year.
5. The object has information about its mass, cross-section, and initial orbit registered in DISCOS.
6. The object did not undergo a fragmentation.
7. At least 10 Two Line Elements (TLEs) are available for the object.

The rationale behind the first two requirements is simply to define the scope of the study to objects that correspond to rocket stages and that are on orbits that interfere with the LEO region. Furthermore, in order to have a reference to assess the accuracy of the orbital lifetime estimations, it was required to analyze only objects with an already known re-entry epoch. The requirement number 4 is intended to discard objects that are not relevant for the study due to having spent too short time orbiting Earth. As the mass, cross-section and initial orbit are required parameters for the orbital lifetime estimation, all objects that did not have this information were discarded. Moreover, a fragmentation event can significantly change parameters such as the mass or the cross section of the object, which are essential for the propagations. Therefore, objects that are known to have undergone such an event, were also discarded from the dataset. Finally, objects that had less than 10 TLEs assigned to them were considered to not be well enough characterized, posing strong difficulties when, for instance, the consistency of their initial orbits had to be checked. Consequently, these objects were also discarded form the studied dataset. A total of 770 objects remained in the dataset for the analysis.

The dynamics of the objects resident in the LEO region, where the decay is mainly influenced by the drag that the bodies experience, strongly differs from the dynamics of HEO orbits, where third body perturbations highly influence the orbital evolution and the decay of the objects. For this reason, the objects whose orbits correspond to each of these groups were analyzed separately. As a result, two separated datasets were studied:

- LEO objects: defined as objects whose apogee altitude is below 2,000 km. A total of 340 objects correspond to this group.
- HEO objects: defined as objects whose apogee is above 2,000 km (and perigee below 2,000 km). A total of 430 objects form this group.

The launch epoch and the distribution of the orbits for each group can be seen in fig. 1 and fig. 2 respectively.

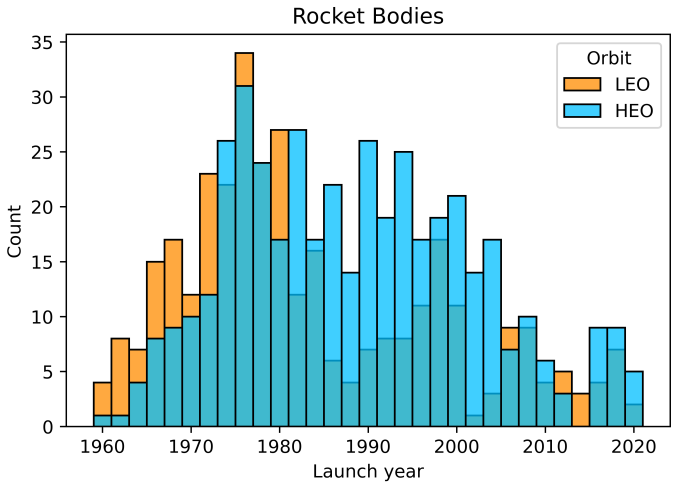

Fig. 1: Distribution of the launch year for the objects in the dataset, separated in LEO and HEO objects.

2.2 Tools

For this study, the tool OSCAR (Orbital SpaceCraft Active Removal) from the DRAMA 3.1.0 (Debris Risk Assessment and Mitigation Analysis) software suite was used, which is the standard tool of the European Space Agency to assess PMD strategies and is freely available online [1]. OSCAR allows to assess the remaining orbital lifetime of an object considering different solar and geomagnetic activity scenarios. It uses a semi-analytical propagator, FOCUS (Fast Orbit Computation Utility Software), which takes singly averaged orbital elements and uses a variable-step multi-step predictor/corrector integrator. In the version used in OSCAR, FOCUS considers geopotential terms up to the 6th order, atmospheric drag using the thermosphere model NRLMSISE-00, third body perturbations caused by the gravitational forces of the Moon and the Sun, and solar radiation pressure (SRP) considering a cylindrical Earth shadow.

[1] https://sdup.esoc.esa.int/

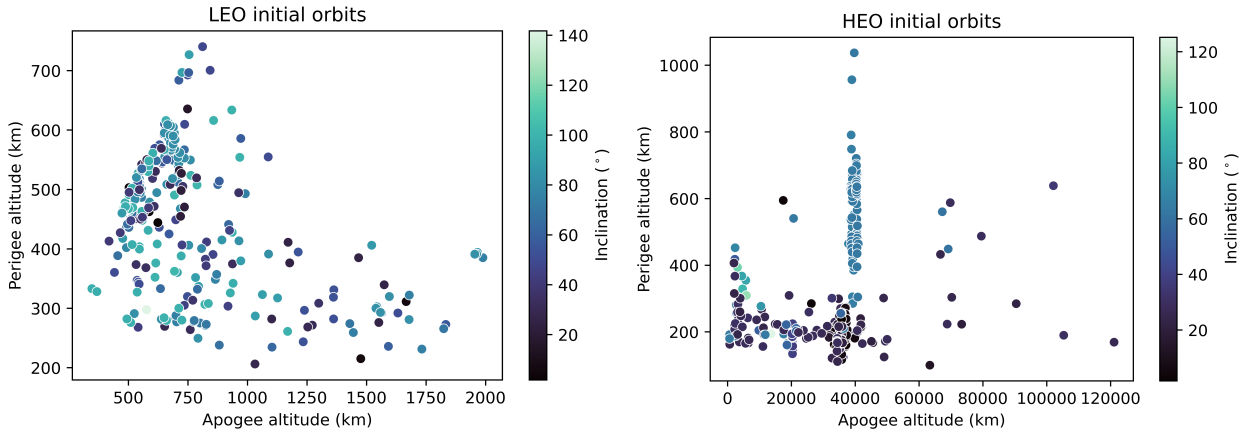

(a) LEO

(b) HEO

Fig. 2: Initial orbits of the objects in the dataset, divided in LEO and HEO objects.

2.3 Procedure

The initial orbits of the objects of the dataset were propagated until their re-entry in order to compare the estimated orbital lifetime with the actual orbital lifetime of the objects. For the LEO objects, the initial orbits registered in DISCOS were used for the propagation. These registered initial orbits include the semimajor axis, the eccentricity, and the inclination of the orbit, as well as the argument of periapsis for some of them. However, the right ascension of the ascending node (RAAN) is typically not included. This is an important parameter for HEO orbits, which are highly influenced by third-body perturbations originated by the Sun and the Moon (also called lunisolar perturbations). Therefore, the first TLE of each of the HEO objects was used as the initial orbit for the propagation. The TLEs used in this study were extracted from [1]. It is also important to note that TLEs include double-averaged orbital elements, while OSCAR takes singly averaged ones. The appropriate conversions were performed with the CState tool, also available in DRAMA.

Also important for the propagation are the physical properties of the propagated objects. In this case, the mass and the average cross-section of the rocket bodies registered in DISCOS were used for the propagation. Furthermore, two different cases were used for the drag coefficient, c_D, of the objects:

1. Using a default $c_D = 2.2$ for all the rocket bodies. This is a very common assumption, as well as the default in OSCAR.
2. Considering that rocket bodies can be approximated as cylinders. The drag coefficient of a randomly tumbling cylinder in a free molecular flow can be calculated as [10]:

$$c_D = 1.57 + 0.785 \cdot \frac{D}{L} \tag{1}$$

Where D is the diameter and L is the length of the cylinder. In this case, the c_D of each rocket body was estimated individually, using the dimensions available on DISCOS.

The propagations for each object were performed for both cases in order to test these two assumptions. Finally, the reflectivity coefficient c_R, which determines the influence of the solar radiation pressure, was kept at a default of $c_R = 1.3$.

When the predicted lifetime of an object differed very strongly from the observed one, both the initial orbit and physical characteristics of the stage were checked in order to detect and correct errors in the database or in the TLE used that could be affecting the propagation. This process reduced significantly the number of outliers in the results. However, it is important to note that the results are still susceptible to underlying errors in the data.

An important factor when the orbit of an object is propagated into the future is the solar and geomagnetic activity considered. Both parameters are important inputs in atmospheric models, strongly influencing the atmospheric density and, therefore, the drag that is experienced by an object. This is of high importance, as the drag force is the main mechanism driving the decay of objects orbiting through the LEO region. Three different scenarios were chosen for this analysis, which are also recommended in [2, 16]:

1. Latest prediction or best guess: in this scenario, the future behavior is estimated based on the current sunspot cycle and based on sampled past cycles [15]. For the past activity, however, the observed solar and geomagnetic activity data is used. As the objects of the dataset used in this paper have already re-entered, the algorithm used the observed solar and geomagnetic activity for the propagations in this scenario. It is important to note that, when a mission and its corresponding disposal are being planned, this will not be the case. Further errors will be introduced then, corresponding to the error in the forecast of the solar and geomagnetic activity.
2. Monte Carlo: the solar and geomagnetic activity used corresponds to this of an equivalent day of the cycle within one of the preceding five solar cycles, which is randomly selected [15].
3. ECSS cycle: this approach consists of repeating the 23rd solar cycle as many times as appropriate for the propagation span, taking into account the position within the solar cycle at the start of the propagation [15].

The outcome of the propagation with OSCAR is a predicted epoch for the re-entry of these objects, and therefore an estimated orbital lifetime. The error in the prediction of the orbital lifetime, E, is defined as the difference between the predicted re-entry epoch x_{pred} and the observed one x_{obs}:

$$E = x_{pred} - x_{obs} \tag{2}$$

This way, a negative error will indicate an underestimation of the orbital lifetime, while a positive error indicates an overestimation of the orbital lifetime. Being L_{obs} the observed orbital lifetime, the relative error e can then be defined as:

$$e = \frac{x_{pred} - x_{obs}}{L_{obs}} \tag{3}$$

3. RESULTS

3.1 LEO

In this subsection, the results obtained for objects resident in the LEO region are shown. The results are shown for three different solar and geomagnetic activity scenarios and for two different assumptions for the drag coefficient, as stated in section 2.

3.1.1 Default drag coefficient $c_D = 2.2$

The results obtained for the objects resident in LEO assuming a default drag coefficient of $c_D = 2.2$ for all rocket bodies are shown in fig. 3. It is important to note that, as it can be understood from eq. (3), a negative error implies that the orbital lifetime of the object is underestimated by the predictions, while a positive error means that the predictions overestimate the lifetime. It can be seen that the distribution of the error is clearly skewed to the left for all solar and geomagnetic activity scenarios. Thus, in these conditions, OSCAR tends to underestimate the orbital lifetime of the rocket bodies.

Table 1 shows the average $\bar{x}$, median $\widetilde{x}$ and standard deviation σ of the relative error. The negative values of both the average and median for all scenarios signal the previously mentioned tendency to underestimate the orbital lifetime. Furthermore, the latest prediction scenario seems to yield the biggest underprediction of all. As the latest prediction scenario uses the observed values of the solar activity, it is not subject to errors originating from the used solar and geomagnetic activity. Therefore, the fact that it shows the largest error of the three solar and geomagnetic activity scenarios signals that errors in the force model, most probably in the atmospheric model and in the ballistic coefficient

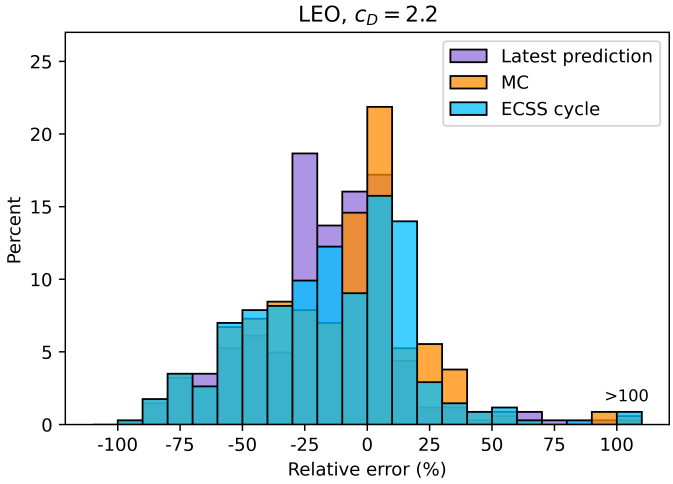

Fig. 3: Relative error of the re-entry predictions for the RBs in LEO using a default drag coefficient of $c_D = 2.2$ and for three different solar and geomagnetic activity scenarios.

	Latest prediction	Monte Carlo	ECSS Cycle
$\bar{x}$ (%)	-17.20	-12.85	-14.61
$\widetilde{x}$ (%)	-16.16	-4.96	-13.04
σ (%)	29.51	33.69	33.02

Table 1: Average, median and standard deviation of the error for the three solar and geomagnetic activity scenarios for the RBs in LEO using the default $c_D = 2.2$.

of the objects, are being compensated by the errors in the solar and geomagnetic activity used in other scenarios.

In order to understand these results, it was important to understand in which period, and more specifically during which solar cycles, the objects in the studied dataset were in orbit. Fig. 4 shows the number of objects of the dataset corresponding to LEO that were orbiting Earth at any time during each solar cycle, as well as the observed F10.7 (monthly average) in Solar Flux Units (SFU). It can be observed that the objects in the studied dataset were predominantly in orbit during cycle 21, which counts around 200 objects while the next cycles have a maximum of 125 objects. The solar activity during solar cycle 21 was higher than for solar cycle 23, which is the ECSS cycle. It can be interpreted that the solar activity used for the propagations in the latest prediction scenario would tend to be higher than in the ECSS cycle, which explains why the lifetime is slightly more underestimated for this scenario. The Monte Carlo scenario, on the other hand, uses cycles 20 to 24, which on average would also imply a weaker solar activity when compared to cycle 21.

3.1.2 Estimated drag coefficient

In this section, the results obtained by using a specific c_D for each rocket body, calculated with eq. (1), are presented. Firstly, the distribution of the calculated drag coefficients is shown in fig. 5. While an accumulation of objects can be observed for values of the c_D between 2.0 and 2.1, reasonably close to the previously assumed 2.2, the biggest peak can be found for values between 1.8 and 1.9. It seems that, generally, the value of 2.2 is overestimating the drag coefficient, which could explain the tendency to underestimate the orbital lifetime observed in fig. 3.

The histograms in fig. 6 show the comparison of the relative error distribution for the two c_D for all the solar and geomagnetic activity scenarios. In the latest prediction scenario, the use of the estimated c_D seems to ”correct” the

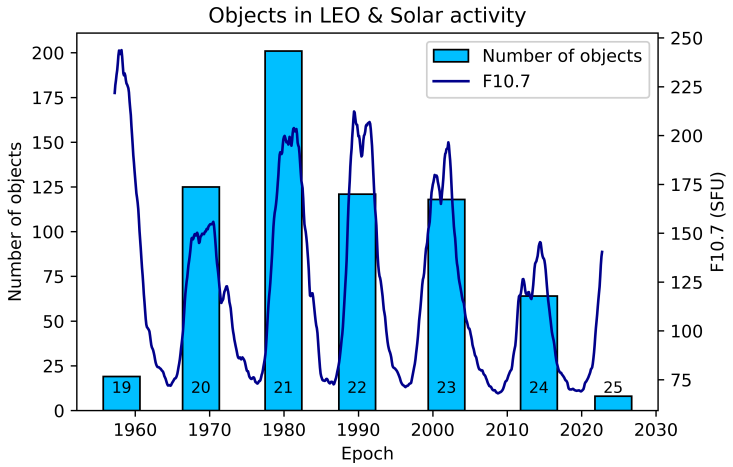

Fig. 4: Number of LEO objects from the dataset that were in orbit during each solar cycle, as well as the monthly solar activity for the studied period. The number at the bottom of each bar represents the solar cycle number for reference.

skewness of the distribution, leading to a seemingly ”normal” distribution centered closely around 0. Table 2 shows that, in this scenario, the mean and the median are really close, and also close to 0, showing a very slight underestimation of the orbital lifetime with an average error close to -3%.

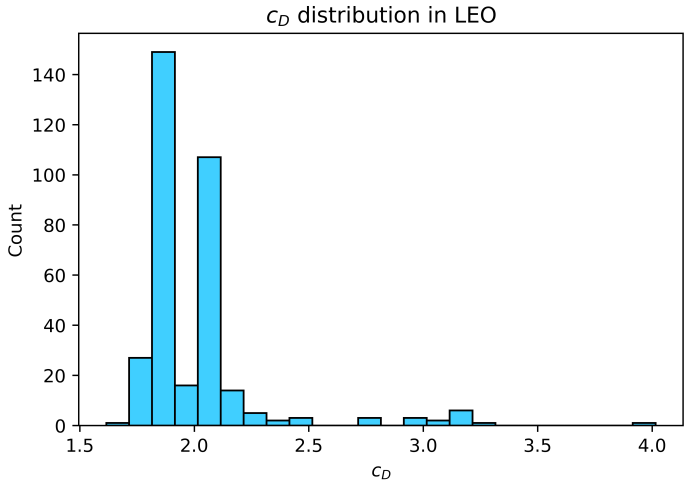

Fig. 5: Distribution of the calculated drag coefficients for the RBs in LEO.

The distribution of the error for the Monte Carlo scenario also shifted towards more positive values. While the left tail of the distribution seems *fatter* than the right one, the peaks between 0-10 % and 10-20% error dominate the distribution, resulting in a slight skewness to the right and consequently overestimating the orbital lifetime. This is also shown by the mean and median shown in table 2.

Finally, the distribution of the error for the ECSS cycle scenario shows even more dominating peaks in the 0-10% and 10-20% error bins, which will be analyzed in more detail in section 3.1.3. Furthermore, the difference between the left and right tails is even more visible than in the Monte Carlo scenario, with a significantly heavier left tail. This turns into a negative mean value of -1.10% error, while the median is more affected by the positive peaks and provides a value of 4.44%.

As the results in the latest prediction scenario showed a clear improvement, correcting the tendency to underestimate the orbital lifetime, and considering that this scenario uses the observed solar and geomagnetic activity, it can be concluded that the assumptions made to estimate the drag coefficient with eq. (1) seem valid, or lead to more accurate results as the default 2.2, for the RBs in the studied dataset.

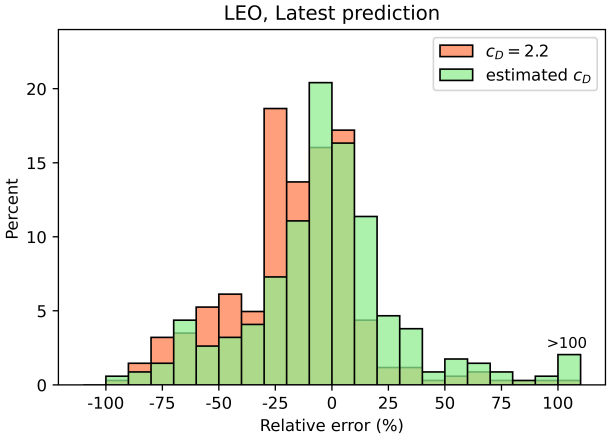

(a) Latest prediction scenario.

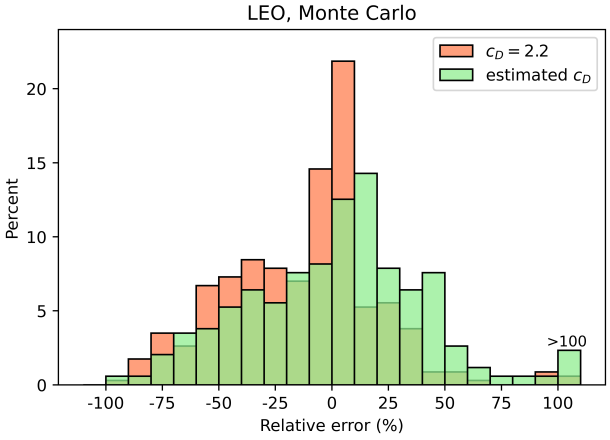

(b) Monte Carlo scenario.

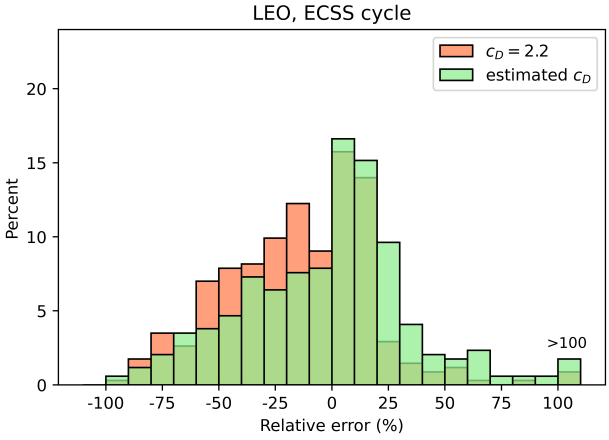

(c) ECSS cycle scenario.

Fig. 6: Comparison of the distribution of the relative error for the two cases for the c_D for each solar and geomagnetic activity scenario.

	Latest prediction	Monte Carlo	ECSS Cycle
$\bar{x}$ (%)	-2.94	2.32	-1.10
$\widetilde{x}$ (%)	-2.74	7.80	4.44
σ (%)	36.31	40.10	38.59

Table 2: Average, median and standard deviation of the error for the three solar and geomagnetic activity scenarios for the RBs in LEO using the estimated c_D.

3.1.3 Error distribution by launch year

An important factor in the way the predictions can differ from the actual orbital evolution and lifetime is the time period in which the studied objects were in orbit, and how much the actual solar and geomagnetic activity differed from the estimated scenarios used. This is especially important for the ECSS cycle scenario, as the solar and geomagnetic activity from a specific cycle, cycle 23, is used. As it can be seen in fig. 4, this cycle has a smaller solar activity than cycles 19, 21 and 22, but a significantly higher solar activity than cycle 24 or cycle 20. This can also be an important factor for the predictions made with the Monte Carlo scenario, which uses cycles 20 to 24. However, it should not make a big difference for the latest prediction scenario, as it uses the observed solar activity data.

While it could be ideal to analyze separately the average error of the objects in each solar cycle, this is not so simple, as most objects are in orbit through more than one solar cycle. Furthermore, taking for instance only the cycle in which they were launched would lead to too small datasets. Therefore, it was chosen to only divide the data in two groups: objects launched before the 1st of August 1996, to take those launched before the start of the ECSS solar cycle, and objects launched afterwards. The groups were not even, with 263 objects in the first group and 77 in the second one, but they were big enough to be representative. The results obtained for each solar and geomagnetic activity scenario are shown in fig. 7 and table 3.

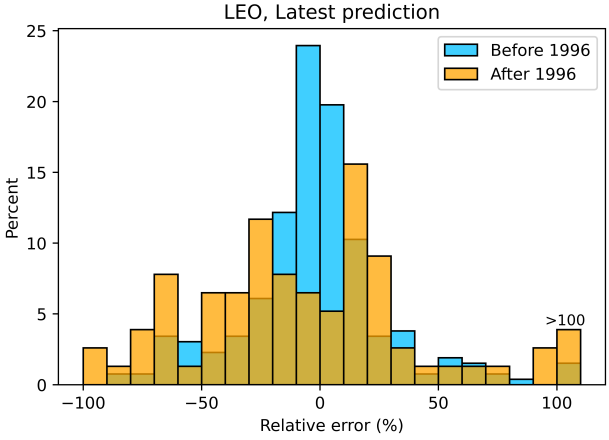

(a) Latest prediction scenario.

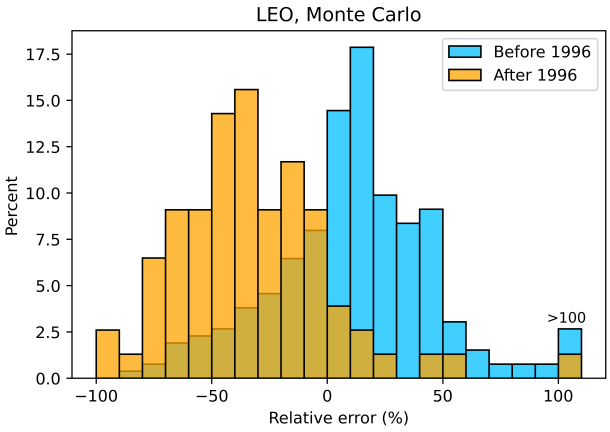

(b) Monte Carlo scenario.

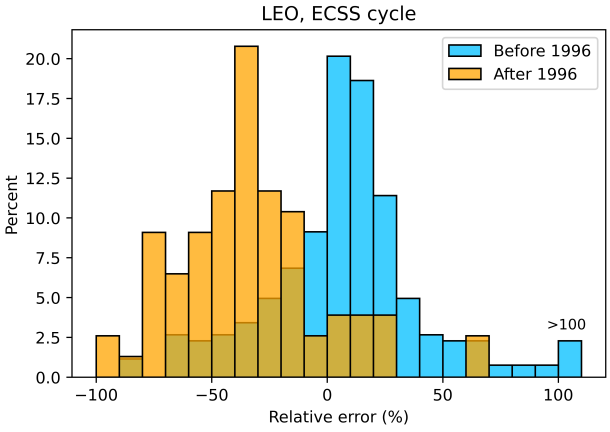

(c) ECSS cycle scenario.

Fig. 7: Distribution of the relative error for each solar and geomagnetic activity scenario, using the estimated c_D, of objects launched before and after the 1st of August 1996.

The most surprising results were obtained for the Monte Carlo and ECSS cycle scenarios, where two completely different distributions can be distinguished. In both cases, two seemingly ”normal” distributions can be distinguished, but centered around a very different value for the objects before and after August 1996. In both cases, the objects launched before the aforementioned date show an overestimation of the orbital lifetime of nearly 10%, while the objects launched afterward show an underestimation of about -30%. This distinct behavior can be explained by the different magnitude of the solar activity during the periods in which these objects were in orbit, while the underlying data used to calculate the solar activity used in the propagations remained the same.

In the latest prediction scenario, the behavior is notably different. While there is no shift between the ”before” and ”after” distributions, the ”after” distribution does not present a strong peak around 0, as is the case for both the ”before” and the complete distribution shown in the previous section. To get a better insight, fig. 8 shows the distribution of the orbital lifetimes for objects launched before and after August 1996. It can be seen that the objects in the latter group tend to have much smaller orbital lifetimes, which would normally lead to larger relative errors. This can explain the different distributions obtained for the two groups in fig. 7a. Furthermore, even though in this scenario there is not uncertainty associated to the estimated solar and geomagnetic activity parameters used, the errors in the atmospheric models are not necessarily uniform for all the ranges of these parameters. If the calibration of the models is less accurate for lower solar activity, for instance, that could also help explain the results in fig. 7a.

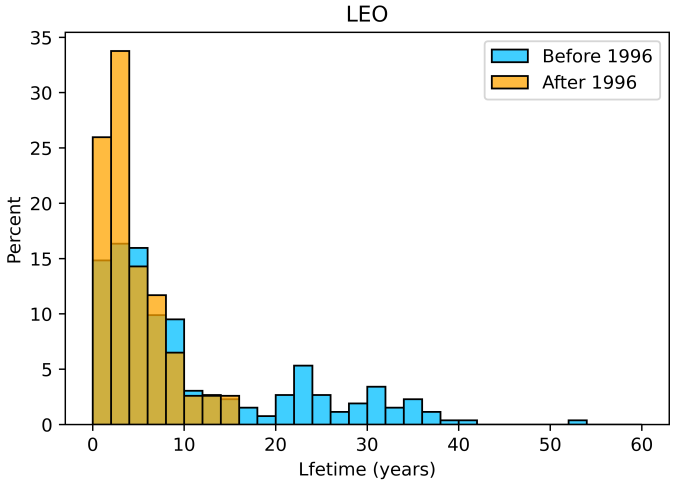

Fig. 8: Distribution of the orbital lifetime for objects launched before and after the 1st of August 1996.

	Latest prediction		Monte Carlo		ECSS cycle	
	Before 1996	After 1996	Before 1996	After 1996	Before 1996	After 1996
$\bar{x}$ (%)	-2.16	-6.77	11.95	-31.78	7.94	-32.98
$\widetilde{x}$ (%)	-2.28	-8.88	12.40	-34.75	9.22	-35.46
σ (%)	31.01	46.71	35.10	34.49	33.71	31.67

Table 3: Average, median, and standard deviation of the relative error for the ECSS cycle scenario, using the estimated c_D, of objects launched before and after the 1st of August 1996.

3.1.4 Long-lived vs short-lived objects

Another important factor to consider when analyzing the error is how long the actual lifetime of these objects is, as a large relative error in an object with a short orbital lifetime has very different implications than the same relative

error for an object with a longer orbital lifetime. Furthermore, it is important to analyze whether different results and dynamics can be expected for short and long-lived objects.

To analyze the actual magnitude of the error, the results shown in fig. 9 are provided in years. As could be expected, short-lived objects present errors with a smaller magnitude than long-lived objects. In all solar and geomagnetic activity scenarios, they present a distribution centered around 0, where the dominant peak is located, with a seemingly small standard deviation and very thin tails. However, the distributions found for long-lived objects are very different. In the latest prediction scenario, the distribution is still clearly centered around 0, and the main difference with respect to the short-lived objects is the tails that extend into larger errors. For the Monte Carlo and the ECSS cycle scenarios, on the other hand, the peak around 0 is much less dominant, leading to distributions with much fatter tails that present further peaks around other error values.

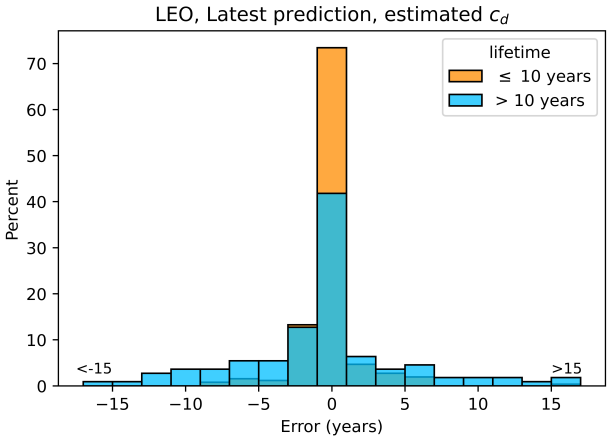

(a) Latest prediction scenario.

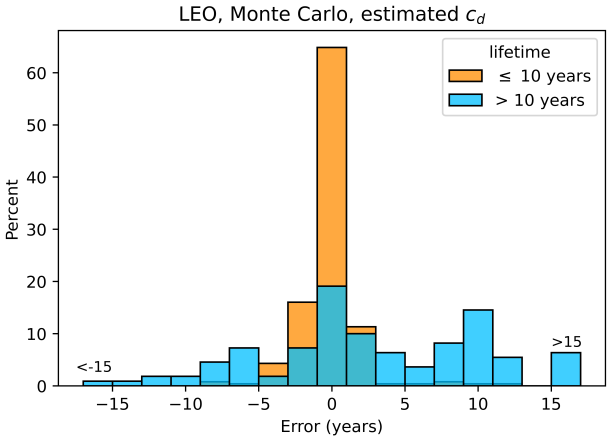

(b) Monte Carlo scenario.

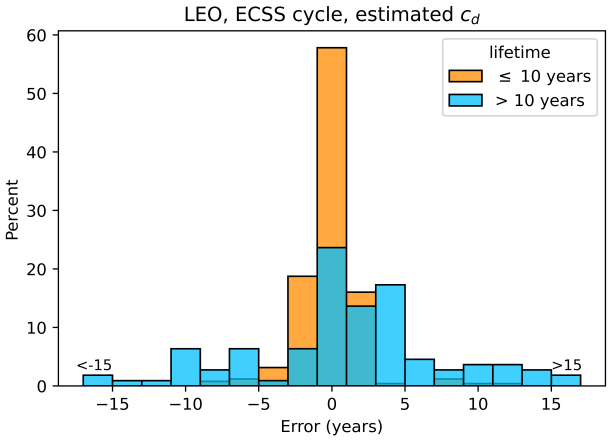

(c) ECSS cycle scenario.

Fig. 9: Comparison of the distribution of the relative error for long and short-lived objects in LEO, using the estimated c_D and for each solar and geomagnetic activity scenario.

An interesting effect can be found when analyzing a significant peak in the distribution of the error of the MC scenario around the 10 years error, as well as around -10 years in the ECSS cycle scenario. Those peaks seem to be related to the solar cycle. For instance, the 10 years error peak corresponds to objects that, in the propagation, did not re-enter around the solar maximum where they re-entered in reality. As the solar activity lowered, the perigee of the object did not go lower into the atmosphere for a long time, until it lowered again close to the next solar maximum and finally re-entered. An example of this effect is shown in fig. 10 where a Cosmos 3 stage with COSPAR-ID 1979-020B

re-enters both in reality and in the latest activity scenario close to the solar maximum of cycle 23, while in the MC and ECSS cycle scenarios, it has to ”wait” until the next solar maximum. The peak around -10 years error, on the other hand, corresponds to objects with the opposite effect,i.e. the propagations consider that they re-enter one solar maximum earlier than in reality.

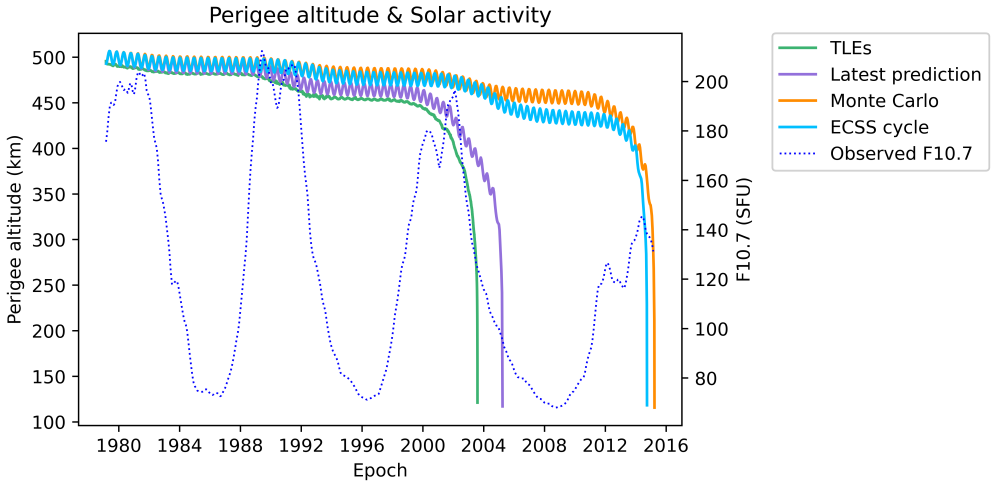

Fig. 10: Evolution of the altitude of the perigee for object 1979-020B for the real case (TLEs) and for the predictions with the three solar and geomagnetic activity scenarios, as well as the observed F10.7 for the studied period.

3.2 HEO

3.2.1 Default drag coefficient $c_D = 2.2$

The results obtained for the objects in HEO assuming a default drag coefficient of $c_D = 2.2$ are shown in fig. 11, with more insight provided in table 4. It can be observed that the distribution of the error for these objects is significantly more spread than for the objects in LEO, featuring also a notably high number of outliers. This is represented by a large standard deviation, as can be seen in table 4. It can be highlighted that the distribution of the error as shown in fig. 12 seems to perform very similarly for all solar and geomagnetic activity scenarios. All cases show a dominant peak in the 0-10% error bin, and a very spread distribution with a fatter left tail than right, which could signal a tendency to underestimate the orbital lifetime. However, the big number of outliers with over 100% error moves the average towards positive values for the three studied scenarios. This is especially due to the presence of objects with errors up to 1,000%, while by definition there cannot be objects with errors below -100%. The median of the distributions, which is less influenced by the outliers, remains close to -6% in all cases.

The large spread of the error distribution, as well as the high number of outliers, were already expected for HEO. This is due to the high sensitivity of these orbits to initial conditions, as previous studies show [11, 14]. An example showing the dynamics that lead to large errors in the orbital lifetime estimation is investigated later in section 3.2.3.

	Latest prediction	Monte Carlo	ECSS Cycle
$\bar{x}$ (%)	3.33	8.17	15.52
$\tilde{x}$ (%)	-5.92	-5.96	-5.71
σ (%)	95.44	183.40	165.38

Table 4: Average, median and standard deviation of the error for the three solar and geomagnetic activity scenarios for the RBs in LEO using the default $c_D = 2.2$.

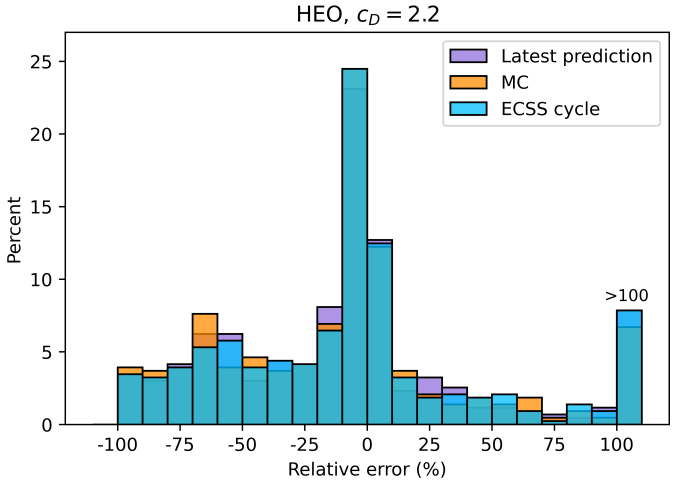

Fig. 11: Relative error of the re-entry predictions for the RBs in HEO using a default drag coefficient of $c_D = 2.2$ and for three different solar and geomagnetic activity scenarios.

3.2.2 Estimated drag coefficient

This section presents the results obtained using a specific c_D for each rocket body, which was estimated using eq. (1) and the dimensions of the stages found in DISCOS. First, the distribution of the calculated drag coefficients can be found in fig. 12. In comparison with the drag coefficients calculated for the LEO objects, higher drag coefficients are present for this set of objects, with a noticeable peak between 2.4-2.5. The other dominant peak, however, is found between 1.7-1.8, while a significant number of objects can still be found between 2.0 and 2.2.

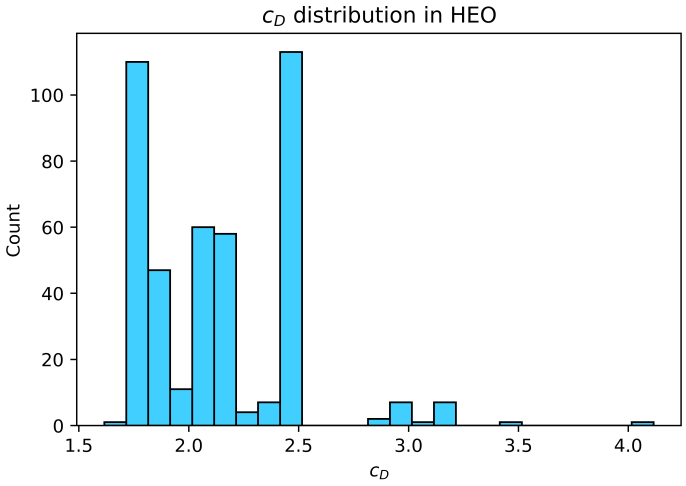

Fig. 12: Distribution of the calculated drag coefficients for the RBs in HEO.

The histograms shown in fig. 13 show the comparison of the relative error distribution for the two c_D cases for all the solar and geomagnetic activity scenarios. As opposed to the results observed in LEO, the use of the estimated c_D does not seem to provoke any important changes in the distribution. This can be explained by the fact that drag is less important for HEO orbits than for LEO, with the former being more affected by luni-solar perturbations. The average, median and standard deviation of the relative error for the estimated c_D case are shown in table 5. Again, the standard deviation and the mean, which are significantly affected by outliers, differ for each scenario, with positive means and very high standard deviations. However, the median falls very close to -5% for all cases.

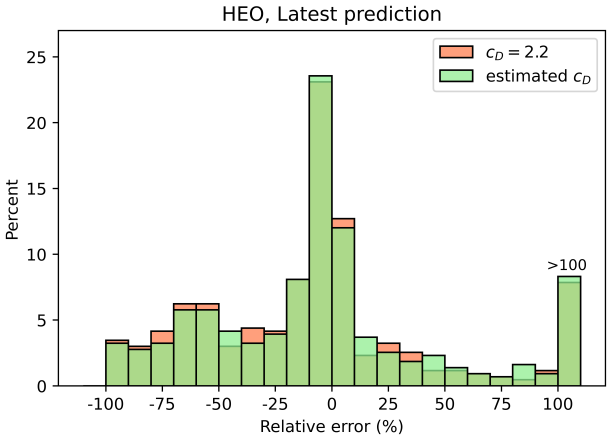

(a) Latest prediction scenario.

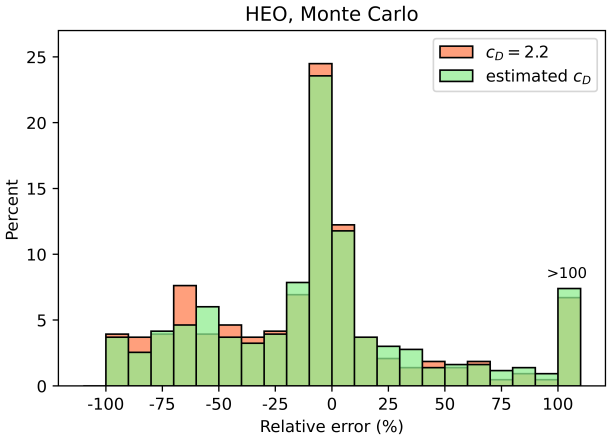

(b) Monte Carlo scenario.

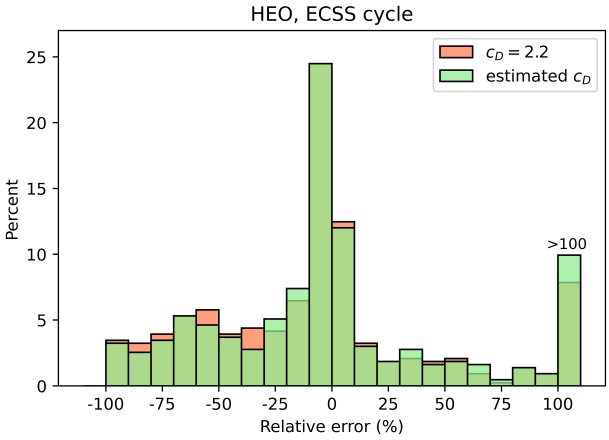

(c) Repeated cycle scenario.

Fig. 13: Comparison of the distribution of the relative error for the two cases for the c_D for each solar and geomagnetic activity scenario.

	Latest prediction	Monte Carlo	ECSS Cycle
$\bar{x}$ (%)	9.20	10.12	18.93
$\tilde{x}$ (%)	-5.17	-4.94	-4.64
σ (%)	126.47	149.34	153.12

Table 5: Average, median and standard deviation of the error for the three solar and geomagnetic activity scenarios for the RBs in HEO using the estimated c_D.

3.2.3 Example stage

The goal of this section is to show one of the effects that make orbital lifetime predictions in HEO so challenging. An example stage has been chosen for the analysis, which corresponds with an H10 stage from an Ariane 4 rocket. More specifically, it is the rocket body with COSPAR-ID 1989-020C. The physical characteristics and initial orbital parameters of this object are shown in table 6. The mass and dimensions of the stage were taken from the launcher manual [5], the average cross section computed using the CROC (Cross Section of Complex Bodies) tool from DRAMA and

the c_D using eq. (1). The orbital parameters were taken from the first TLE of the object and transformed into singly averaged elements with CState. This stage was launched on 1989-03-06 and re-entered on 1992-04-21, with a total of 3.12 years lifetime. However, the re-entry predictions resulted as follows in table 7, with their corresponding errors. Furthermore, the evolution of the semimajor axis is shown in fig. 14.

Mass (kg)	Cross-section (m^2)	c_D	a (km)	e	i (°)	Ω (°)	ω (°)	epoch
1780	26.76	1.77	24,617.81	0.7337	6.89	332.05	177.10	1989-03-08 02:41:03

Table 6: Physical characteristics and initial orbit of object 1989-020C. The nomenclature used is as follows: a represents the semimajor axis, e the eccentricity, i the inclination, Ω the right ascension of the ascending node and ω the argument of perigee.

Scenario	Re-entry epoch	Error (years)	Relative error (%)
Latest prediction	1994-12-16	2.65	84.93
Monte Carlo	1997-03-13	4.89	156.66
ECSS Cycle	2011-12-20	19.66	629.48

Table 7: Orbital lifetime predictions and errors for object 1989-020C for the different solar and geomagnetic activity scenarios using the data in table 6

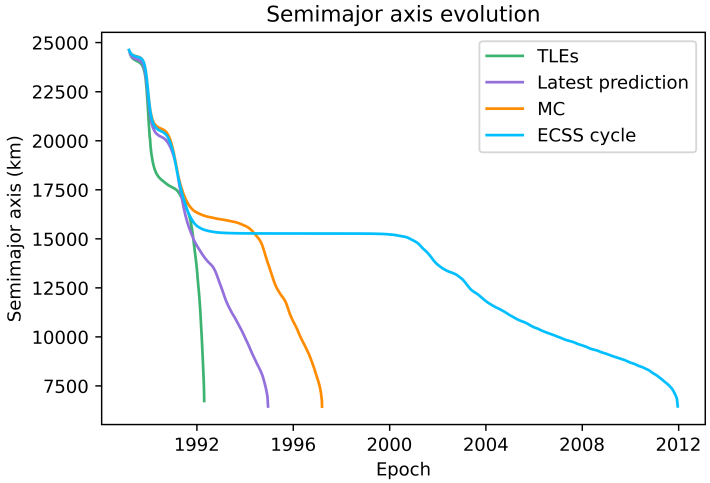

Fig. 14: Evolution of the semimajor axis of object 1989-020C for all the solar and geomagnetic activity scenarios, as well as the real evolution based on TLE data.

As it can be seen in table 7 and fig. 14, the re-entry predictions for this object have a large error. It is especially important to highlight the large difference between the predictions obtained for the different scenarios, with about 17 years difference between the latest prediction and the ECSS cycle scenario.

It is important to understand how drag influences the decay of these eccentric objects. When the perigee is deep into the atmosphere, the object experiences the drag force when it is close to the perigee. The drag force ”slows down” the object, decreasing the energy of the orbit and therefore the semimajor axis, circularizing the orbit. For this reason, the altitude of the perigee is a very important factor in the decay of HEO objects, as it will determine how much drag the object experiences.

An important factor in the evolution of the perigee altitude is the orientation of the orbit with respect to the Sun, described by the right ascension of the Sun in the orbital plane α, which determines if the gravity of the Sun drives the perigee up or deeper into the atmosphere. More specifically, when $0^\circ < \alpha < 90^\circ$ or $180^\circ < \alpha < 270^\circ$, the perigee altitude increases, delaying the re-entry, and when $90^\circ < \alpha < 180^\circ$ or $270^\circ < \alpha < 360^\circ$, the perigee altitude decreases, accelerating the re-entry [8, 6].

Furthermore, the evolution of the semimajor axis and eccentricity in a drag affected orbit can sometimes lead to sun-synchronous conditions. Thus, the precession of the right ascension of the ascending node of the orbit Ω and the argument of perigee ω are such that the orientation of the orbit with respect to the Sun is maintained. This condition can be sustained for long periods. If this phenomenon takes place when α is such that the perigee altitude is increasing, it can be driven to very high altitudes, which will greatly delay the re-entry. This effect is referred as sun-synchronous resonance [8, 6].

This effect is shown in fig. 15. The plot shows the evolution of the sun angle and the evolution of the perigee for the three solar and geomagnetic activity scenarios and the actual evolution based on TLE data, for the period between the launch and 1996. Moreover, fig. 16 shows the evolution of the same parameters corresponding only to the ECSS cycle scenario and the TLE data until the predicted re-entry according to this scenario, in order to show the evolution of the worst case. The horizontal lines are placed at 180° and 270° to show the limits of the quadrant of interest. In this quadrant, the altitude of the perigee increases. It can be seen that, for the actual evolution of the orbit of this object between 1991 and 1992, the Sun angle does not enter this quadrant and thus the perigee altitude decreases. However, this is not the case for the predicted trajectories. All of them enter this quadrant, which explains the large error in the predictions as the perigee altitude increased for a certain period of time. Moreover, the differences in the solar activity scenarios and therefore in the evolution of the semimajor axis and eccentricity lead to sun-synchronous conditions (or nearly) reached in two of the scenarios, Monte Carlo and ECSS cycle.

The latest prediction scenario presents a rather fast pass through this quadrant, leading to over 2.5 years error in this scenario. Even though the orientation with respect to the sun in the Monte Carlo scenario did not reach constant conditions, the evolution of the sun angle got significantly slower, with about 2 years spent in this quadrant and a more significant increase of the perigee altitude that led to almost 5 years error in this scenario. Finally, the ECSS cycle scenario does present a period in which the sun angle remains apparently constant; thus, it reaches sun-synchronous conditions. In this case, the perigee altitude keeps increasing for about 5 years, reaching values above 500 km. This caused an error of almost 20 years in the predictions.

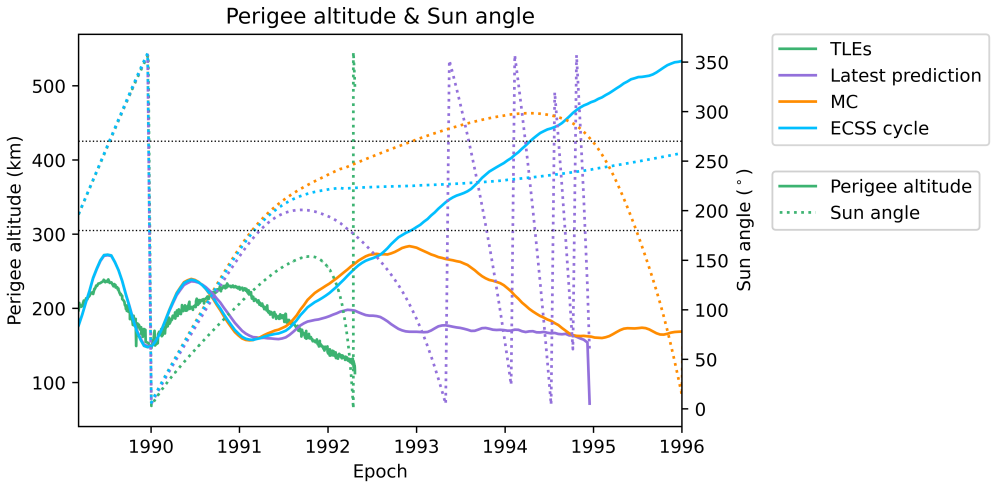

Fig. 15: Evolution of the sun angle and evolution of the perigee of object 1989-020C for the three solar and geomagnetic activity scenarios and the actual evolution based on TLE data, for the period between the launch and 1996.

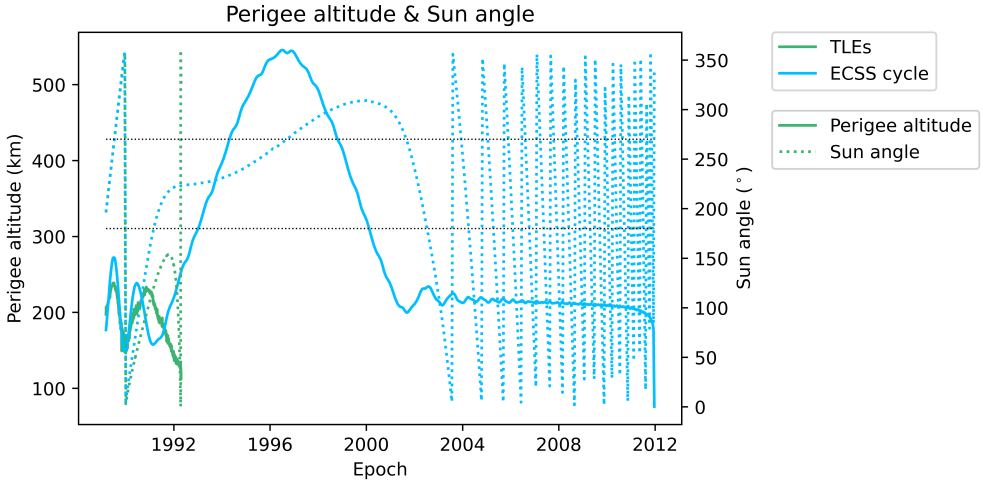

Fig. 16: Evolution of the sun angle and evolution of the perigee of object 1989-020C for ECSS cycle scenario and TLE data.

4. CONCLUSIONS

The paper has shown an in-depth analysis of the errors obtained in the orbital lifetime predictions of 770 RBs, divided into two datasets corresponding to two distinct orbital regimes, LEO and HEO. The main factors influencing the predictions in both regimes have been analyzed, and the main dynamics leading to large errors described. Despite the comprehensive analysis that this paper intends to give, many questions remain a subject for future analyses.

The results in LEO were satisfactory for the latest prediction scenario. However, in this paper, this scenario could use the data available of actually observed solar and geomagnetic activity data. Therefore, the uncertainties introduced by the use of forecasted parameters still need to be assessed. Moreover, it was seen that the use of a specifically calculated drag coefficient significantly improved the results. Future analysis will assess how the predictions can be improved using better estimations of the ballistic coefficient.

The results in HEO showed that orbital lifetime estimations in this region are still very challenging. Future analyses will assess the impact of using a different propagator. It will also be investigated whether propagating an initial set of TLEs, instead of only the first one, can lead to improved estimations. Furthermore, [11] suggests that statistical methods are required to assess orbital lifetimes in these orbits, which shall also be explored.

ACKNOWLEDGEMENTS

The project leading to this application has received funding from the European Union's Horizon 2020 research and innovation programme under the Marie Skłodowska-Curie grant agreement No 860956.

REFERENCES

[1] https://www.space-track.org/.
[2] International Standard ISO 24113, Space systems - space debris mitigation requirements. Technical report, ISO, July 2019.
[3] IADC space debris mitigation guidelines. Technical report, Inter-Agency Space Debris Coordination Committee, March 2020.

[4] European Space Agency. *Position Paper on Space Debris Mitigation, Implementing Zero Debris Creation Zones (ESA SP-1301)*. ESA Publications Division, 2004.
[5] Arianespace. *ARIANE 4 user's manual, Issue n°2, Rev. 0*, February 1999.
[6] F. Bonaventure, S.lim Locoche, and A. H. Gicquel. De-orbitation studies and operations for spirale gto satellites. *Proceedings 23rd InternationalSymposium on Space Flight Dynamics, Passadena, California*, 2013.
[7] V. Braun, S. Lemmens, H. Krag, T. Flohrer, K. Merz, B. Bastida Virgili, and Q. Funke. Probabilistic orbit lifetime assessment with oscar. *Proceedings of 6th International Conference on Astrodynamics Tools and Techniques (ICATT)*, 2016.
[8] E. David and V. Braun. Re-entry analysis comparison with different solar activity modelsof spent upper stage using ESA's drama tool. *6th IAASS Conference Proceedings*, 2013.
[9] V. Braun; S. Lemmens; B. Reihs; H. Krag; A. Horstmann. Analysis of breakup events. In *7th European Conference on Space Debris*, April 2017.
[10] R. D. Klett. Drag coefficients and heating ratios for right circular cylinders in free-molecular and continuum flow from mach 10 to 30. Technical report, Sandia Coorporation, Aerospace Nuclear Safety Reserach Report, 1964.
[11] C. Le Fèvre, H. Fraysse, V. Morand, A. Lamy, C. Cazaux, P. Mercier, C. Dental, F. Deleflie, and D.A. Handschuh. Compliance of disposal orbits with the french space operations act: The good practices and the stela tool. *Acta Astronautica*, 94(1):234–245, 2014.
[12] ESA Space Debris Office. ESA's annual space environment report. Technical report, European Space Agency (ESA), 2023.
[13] A. Operti, V. Braun, S. Lemmens, and S. Corpino. Assessing uncertainties in the estimation of the orbital lifetime. *Proceedings 7th European Conference on Space Debris*, 2017.
[14] D. K. Skoulidou, A. J. Rosengren, K. Tsiganis, and G. Voyatzis. Dynamical lifetime survey of geostationary transfer orbits. *Celestial Mechanics and Dynamical Astronomy*, 130(77), 2018.
[15] J. Gelhaus C. Kebschull S. Flegel M. Möckel C. Wiedemann H.Krag P. Vörsmann V. Braun, N. Sánchez-Ortiz. Upgrade of the esa drama oscar tool: Analysis of disposalstrategies considering current standards for future solar andgeomagnetic activity. *Proceedings: '6th European Conference on Space Debris'*, 2013.
[16] ESA Space Debris Mitigation WG. ESA space debris mitigation compliance verification guidelines. Technical report, European Space Agency, February 2015.